ADVANCED MATERIALS
www.advmat.de

Electrically Insulating Flexible Films with Quasi-1D van der Waals Fillers as Efficient Electromagnetic Shields in the GHz and Sub-THz Frequency Bands

*Zahra Barani, Fariborz Kargar, Yassamin Ghafouri, Subhajit Ghosh, Konrad Godziszewski, Saba Baraghani, Yevhen Yashchyshyn, Grzegorz Cywiński, Sergey Rumyantsev, Tina T. Salguero, and Alexander A. Balandin**

Polymer composite films containing fillers comprising quasi-1D van der Waals materials, specifically transition metal trichalcogenides with 1D structural motifs that enable their exfoliation into bundles of atomic threads, are reported. These nanostructures are characterized by extremely large aspect ratios of up to ≈10^6. The polymer composites with low loadings of quasi-1D $TaSe_3$ fillers (<3 vol%) reveal excellent electromagnetic interference shielding in the X-band GHz and extremely high frequency sub-THz frequency ranges, while remaining DC electrically insulating. The unique electromagnetic shielding characteristics of these films are attributed to effective coupling of the electromagnetic waves to the high-aspect-ratio electrically conductive $TaSe_3$ atomic-thread bundles even when the filler concentration is below the electrical percolation threshold. These novel films are promising for high-frequency communication technologies, which require electromagnetic shielding films that are flexible, lightweight, corrosion resistant, inexpensive, and electrically insulating.

Z. Barani, Prof. F. Kargar, S. Ghosh, S. Baraghani, Prof. A. A. Balandin
Nano-Device Laboratory (NDL) and Phonon Optimized Engineered Materials (POEM) Center
Department of Electrical and Computer Engineering
University of California, Riverside
Riverside, CA 92521, USA
E-mail: balandin@ece.ucr.edu

Y. Ghafouri, Prof. T. T. Salguero
Department of Chemistry
University of Georgia
Athens, GA 30602, USA

Dr. K. Godziszewski, Prof. Y. Yashchyshyn
Institute of Radioelectronics and Multimedia Technology
Warsaw University of Technology
Warsaw 00-665, Poland

S. Baraghani, A. A. Balandin
Materials Science and Engineering Program
University of California, Riverside
Riverside, CA 92521, USA

Prof. Y. Yashchyshyn, G. Cywiński, Dr. S. Rumyantsev
CENTERA Laboratories
Institute of High-Pressure Physics
Polish Academy of Sciences
Warsaw 01-142, Poland

G. Cywiński
CEZAMAT
Warsaw University of Technology
Warsaw 02-822, Poland

The ORCID identification number(s) for the author(s) of this article can be found under https://doi.org/10.1002/adma.202007286.

DOI: 10.1002/adma.202007286

The explosive growth of interest in 2D layered van der Waals materials, such as graphene and transition metal dichalcogenides (TMDs) MX_2, where M = transition metals and X = S, Se, Te, has resulted in numerous breakthroughs in physics and is expected to lead to important practical applications.[1–5] Recently, a different group of layered van der Waals materials with quasi-1D crystal structures has attracted significant attention: the transition metal trichalcogenides (TMTs). These compounds contain 1D motifs comprised of MX_3 atomic chains that are weakly bound together by van der Waals forces or chalcogen interactions. Examples of such materials include TiS_3, NbS_3, $TaSe_3$, and $ZrTe_3$.[6–13] MX_3 materials exfoliate into nanowire- and nanoribbon-type structures, as opposed to atomic planes of quasi-2D van der Waals MX_2 materials. We previously discovered that bundles of quasi-1D $TaSe_3$ atomic threads and $ZrTe_3$ nanoribbons can support high current densities of $J_B \approx 10$ MA cm^{-2} and $J_B \approx 100$ MA cm^{-2}, respectively.[6,7,14] In this group of MX_3 materials, $TaSe_3$ is particularly interesting. Reported studies generally agree that it is a metal, with superconducting properties at low temperature, although some studies suggest that it is a semimetal.[15–18] The exact band and specifics of electron transport in bulk and exfoliated nanowires of $TaSe_3$ at various temperatures are still under intensive debate.

In this letter, we demonstrate that quasi-1D van der Waals materials like $TaSe_3$ can be used as the high-aspect-ratio metallic fillers in polymer composites to provide important functionality—efficient electromagnetic interference (EMI) shielding—in a wide frequency range that is relevant to current 5G and future communication technologies: X-band (f = 8.2–12.4 GHz) and the extremely high frequency (EHF) band (f = 220–320 GHz). Proliferation of portable devices and wireless communications has led to problems with environmental electromagnetic pollution. There is a need for more efficient EMI shielding materials characterized by low-weight, mechanical stability, resistance to oxidation, flexibility, and ease of manufacturing. Many applications also require EMI shielding films to be electrically insulating to avoid short circuiting of electronic components. The conventional materials for EMI shielding are metals, which are utilized as coatings and enclosures.[19] Metals have charge carrier concentrations

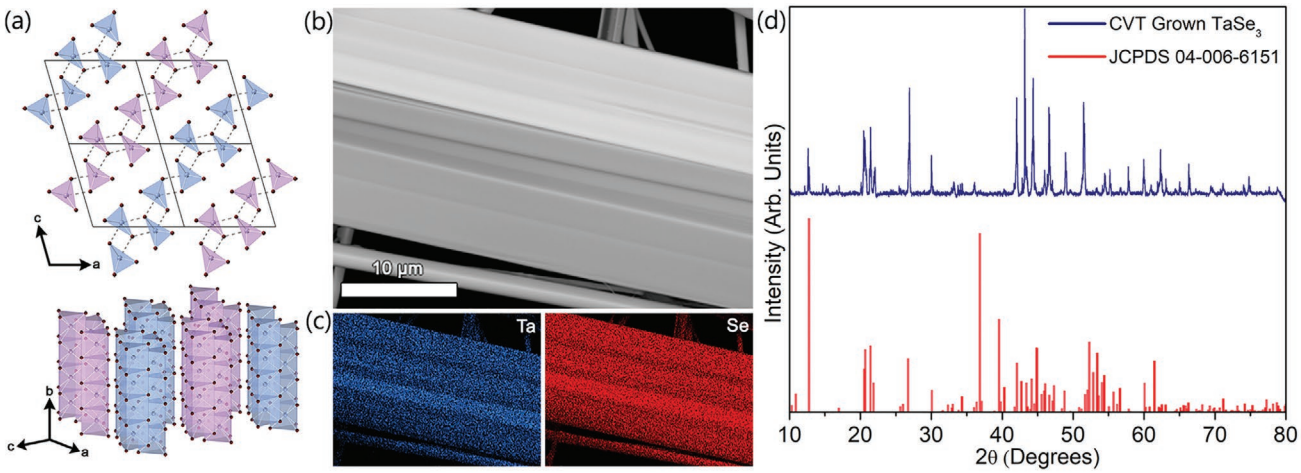

Figure 1. Structure and composition of as-synthesized $TaSe_3$. a) Crystal structure of $TaSe_3$; red spheres represent Se and blue/purple spheres represent Ta. The parallelograms in the top panel outline unit cells viewed along the *b*-axis, perpendicular to the $TaSe_3$ chains. The side view in the bottom panel shows the quasi-1D nature of trigonal prismatic [$TaSe_6$] units extending along the *b*-axis. The corrugated bilayer nature of this structure is emphasized with the Ta···Se interchain interactions and the blue/purple coloring; bilayers are separated from their neighbors by van der Waals gaps. b) SEM image of a mechanically exfoliated $TaSe_3$ crystal. c) Corresponding EDS mapping showing uniform overlap of Ta and Se along the length of the crystal. d) Powder XRD pattern of CVT-grown $TaSe_3$ crystals (blue) matching a reference pattern of monoclinic $TaSe_3$ (red).

that enable them to block EM waves mostly by reflection. However, metallic EMI shields are heavy and prone to oxidation. An alternative approach to EMI shielding is based on the use of polymers containing electrically conductive fillers.[20–23] The first generation of polymer composites for EMI shielding utilized large loading fractions of metallic particles, such that their concentrations are above the electrical percolation threshold, resulting in overall electrically conductive films. The high loading fraction of metallic fillers is required to provide sufficient EMI shieling at a given thickness of the film. Recently, attention has turned to carbon allotrope fillers, including carbon nanotubes and graphene, and transition metal carbide fillers, referred to as MXenes.[21,24–29] For example, we demonstrated efficient EMI shielding in the wide GHz and sub-THz frequency ranges with high-loading graphene composites.[30,31] The advantages of quasi-2D graphene fillers include low weight, high thermal stability, anticorrosive properties, and low cost at mass production. Composites with metallic-like fillers of MXenes typically require high loadings. Such electrically conductive composite has shown to provide efficient EMI shielding in the X-band frequency range.[21] Here, we demonstrate that quasi-1D van der Waals materials can be used as efficient fillers for EMI shielding that, in certain aspects, outperform their quasi-2D counterparts. The synthesized composites and films with quasi-1D van der Waals fillers remain electrically insulating—a desired characteristic for many practical applications.

For experiments with quasi-1D fillers in electrically insulating films for EM shielding, we selected $TaSe_3$. This quasi-1D van der Waals material is well-suited for this application due to its metallic electronic structure and good stability with respect to oxidation. The fact that this material revealed extremely high current densities when exfoliated into the bundles of atomic threads was an additional important factor.[6] Recent interest in $TaSe_3$ has included studies of its topological phases,[17,32–34] the effect of strain on its metallic versus semiconducting states,[35] low temperature charge density wave (CDW) states,[18] and our own work characterizing its current carrying capacity and low-frequency electronic noise.[36] The room temperature, monoclinic crystal structure of $TaSe_3$ (**Figure 1**a) exhibits aligned chains of trigonal prismatic [$TaSe_6$] units oriented along the *b*-axis.[37] These chains are assembled into corrugated bilayers (sets of blue and purple chains in Figure 1a) through Ta···Se interactions between adjacent chains. Neighboring bilayers are separated by van der Waals gaps.

The bulk, crystalline $TaSe_3$ used in this work was prepared by iodine-mediated chemical vapor transport (CVT) from the elements. A temperature gradient of 750 to 650 °C (source zone–growth zone) led to efficient crystal growth during a 2-week period. $TaSe_3$ crystals grew preferentially along the *b*-axis, leading to ribbon- or needle-like, filamentary morphologies ranging from less than one micrometer to tens of micrometers in width (Figure 1b,c; also see Figure S1a,b in the Supporting Information for growth and optical images of the fillers as synthesized). The scanning electron microscopy (SEM) image in Figure 1b shows a $TaSe_3$ crystal that was freshly mechanically exfoliated for energy dispersive spectroscopy (EDS) analysis. EDS mapping shows excellent overlap of Ta and Se (Figure 1c), and quantitative EDS averaged across the entire mapped area (Supporting Information) provides a slightly Se-deficient composition of $TaSe_{2.85}$ similar to other samples prepared by CVT (see Table S1 in the Supporting Information for the details).[6,34] Powder X-ray diffraction (XRD) is consistent with the anticipated monoclinic $TaSe_3$ structure, and it confirms the phase purity of the as-prepared material (Figure 1d).

The preparation of composites with quasi-1D fillers involved chemical phase exfoliation and inclusion of high-aspect-ratio exfoliated threads into three polymeric matrices of sodium alginate (SA), epoxy, and a special type of UV-light-cured polymer (UV-polymer) as the base. The $TaSe_3$ crystals were subjected to solvent-assisted exfoliation separately in two different solvents of acetone and dimethylformamide (DMF). During this process,

the bulk $TaSe_3$ (**Figure 2**a–c) was dispersed and exfoliated in the solvents using low power ultrasonic bath sonication. The dispersion was centrifuged to isolate the solids, and the procedure of sonication/centrifugation was repeated several times. The details of the sample preparation and characterization are provided in the Experimental Section and Figures S2–S4 in the Supporting Information). A photograph of the resultant dispersion is shown in **Figure 2**d. The SEM image in Figure 2e shows the size and morphology of $TaSe_3$ nanowires post-exfoliation. The typical diameter of the exfoliated bundles of the atomic threads of $TaSe_3$ ranges from 50 to 100 nm while their length is in the range of several hundred micrometers. The fillers were mixed with UV-polymer, epoxy, and SA. We tested several different polymers to assess the compatibility of $TaSe_3$ fillers with the embedding polymer matrices and the ability to form thick and thin flexible samples. The obtained flexible

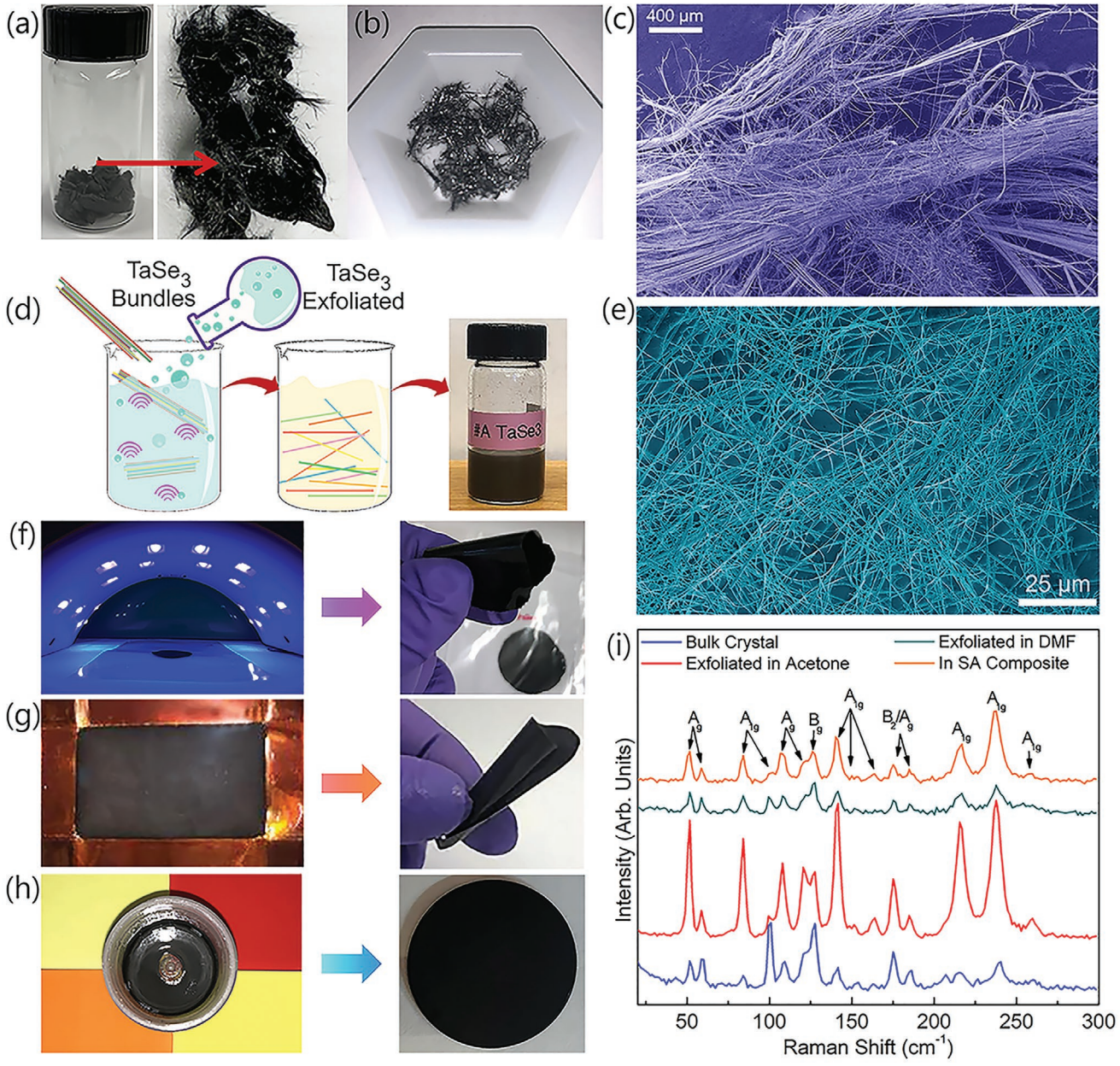

Figure 2. Composite films preparation and characterization. a,b) As-prepared $TaSe_3$ crystals and fibers. c) SEM image of fibrous $TaSe_3$ bundles. d) Schematic showing the process of chemical liquid-phase exfoliation using low-power bath sonication. The vial contains exfoliated $TaSe_3$ in acetone. e) SEM image of $TaSe_3$ threads after liquid-phase exfoliation in acetone. Note the high aspect ratio morphologies. f,g) Synthesis of flexible polymeric films using a special UV-cured polymer (f) and sodium alginate (g) as the matrix and exfoliated $TaSe_3$ as filler. h) Optical image of the 1 mm thick epoxy composite containing about 1.3 vol% concentration of exfoliated $TaSe_3$ threads. i) Raman spectra of the $TaSe_3$ before (blue) and after solvent-assisted exfoliation in acetone (red) and DMF (cyan). The orange curve shows the Raman spectrum of the $TaSe_3$ filler mixed with sodium alginate (SA). The characteristic Raman peaks of $TaSe_3$ do not change as it is exfoliated or combined with SA polymer. Pseudocolors are used in SEM images for clarity.

thin films and composites are shown in Figure 2f–h. Raman spectra of $TaSe_3$ were taken before and after exfoliation in different solvents, and after mixing with the polymer matrix to confirm the quality and stability of the quasi-1D $TaSe_3$ fillers. The measurements were performed in the backscattering configuration under $\lambda = 488$ nm laser excitation using low power to prevent local heating. These results are shown in Figure 2i. The spectrum displays characteristic peaks between 25 and 300 cm^{-1}, which originate from the primitive monoclinic structure of $TaSe_3$.[18,34,35] The peaks at 140, 164, 214, and 238 cm^{-1} are assigned to the out-of-plane A_{1g} phonon modes whereas the peaks at 176 and 185 cm^{-1} to the B_2/A_g modes.[35] The Raman data confirm the crystalline nature of the $TaSe_3$ filler and the preservation of its structural integrity after all processing steps.

To determine EMI characteristics, we measured the scattering parameters, S_{ij}, using a two-port programmable network analyzer (PNA, Keysight N5221A; see the Experimental Section and Figure S5 in the Supporting Information). The scattering parameters define the EM coefficients of reflection, $R = |S_{11}|^2$, and transmission, $T = |S_{21}|^2$, which, in turn, allow one to calculate the coefficient of absorption, A, as $A = 1 - R - T$. A fraction of the energy of EM wave, incident on the film, is reflected at the interface. The rest is absorbed inside the film or transmitted through it. Because part of EM energy is reflected from the interface, the coefficient of absorption, defined as the power percentile of the absorbed EM wave in the medium to the total power of incident wave, is not truly indicative of material's ability in absorbing the EM waves. For this reason, the effective absorption coefficient, A_{eff}, is defined as $A_{\text{eff}} = (1 - R - T)/(1 - R)$. The plots of R, A, and T for all the samples are presented in Figure S6 in the Supporting Information. The total shielding effectiveness, SE_T, describes the total attenuation of the incident EM wave by the material of interest. This parameter determines the material's ability to block the EM waves and consists of two terms—the reflection shielding effectiveness, SE_R, and the absorption shielding effectiveness, SE_A. The latter coefficient includes possible internal reflection as the EM wave passes through the composite medium. These parameters can be calculated in terms of R, T, and A_{eff} as follows: $SE_R = -10\log(1 - R)$, $SE_A = -10\log(1 - A_{\text{eff}})$, and $SE_T = SE_R + SE_A$ (see Section VI in the Supporting Information for details.) The reflection, absorption, and the total EMI shielding effectiveness of the UV-cured flexible polymer films with low concentrations of $TaSe_3$ fillers are presented in **Figure 3**a–c. As one can see, a thin film with 130 μm thickness and an extremely low concentration of 1.14 vol% of quasi-1D $TaSe_3$ fillers reveal strong EMI shielding of ≈10 dB, i.e., 90% of the incident EM power on the film is shielded via reflection at the air–composite interface or absorption as it passes through the composite. Typically, the EMI shielding effectiveness increases with the increasing filler loading.

One can see from Figure 3i that ≈20 dB of total EMI shielding at $f = 8.2$ GHz can be achieved in 27 μm thick SA-based films with only 4.5 vol% of quasi-1D van der Waals fillers. The shielding due to the absorption of EM waves is approximately twice as much as that due to the reflection of the waves. The total EMI shielding effectiveness SE_T, which indicates how much EM energy is blocked by a film of a particular thickness, is not the only characteristic that has to be considered for practical purposes. Another commonly used metric is the effectiveness normalized by the mass density, $SSE = SE_T/\rho$. However, SSE does not fully describe the EMI shielding of a given material because, by increasing the thickness of a film at a constant mass density, one can achieve higher and higher SSE values. To better describe the EMI shielding at the material level, one can normalize SSE by the thickness, t, and use SSE/t to compare the effectiveness of different composites.[21,38] Here, we argue that, for many practical purposes, it is meaningful to normalize $SSE/t = SE_T/(\rho \times t)$ by the loading fraction of the fillers. Achieving higher EMI shielding in the composite with the lowest loading of the fillers makes sense from the weight and cost considerations as well as for maintaining electrical insulation of the composite when required. Indeed, if one composite can deliver the required SE with a low loading of lightweight fillers while another needs 90% loading of silver (Ag) particles, it is clear that the Ag composite likely will be heavy, expensive, and electrically conductive.

To assess the performance of the polymeric composites with fillers, we define the figure-of-merit $Z_B = SE_T/(\rho \times t \times m_f)$ by introducing normalization by the mass fraction of the fillers $m_f = M_F/(M_B + M_F)$, where M_F and M_B are the masses of the filler and the base polymer, respectively. It is interesting to note that the physical meaning of the Z_B figure-of-merit is the total shielding effectiveness of the films per the areal density of the fillers, i.e., $Z_B = SE_T/(M_F/A)$, where $A = V/t$ is the area of the sample of the volume V and thickness t (see the Supporting Information for the details of the derivation). The defined metric put more emphasis on the material performance, and specifically the filler performance. **Figure 4**a,b shows the SSE/t and Z_B for several polymer composites with different fillers. One can see that our composites with quasi-1D van der Waals fillers outperforms composites with carbon nanotubes and graphene. Although a composite with Ag has better performance in terms of SSE/t, the composites with quasi-1D fillers exhibit superior Z_B efficiency. The latter means that the polymer composites with low areal density of quasi-1D fillers are extremely effective in blocking EM waves.

As the next step, we examined the EMI shielding effectiveness of the composites with the low loading of quasi-1D $TaSe_3$ fillers in the EHF band. The measurements were performed using the quasi-optical free space method. The details of the experimental procedures are described in the Experimental Section. **Figure 5**a presents the results of shielding effectiveness of pristine epoxy. As expected, epoxy by itself is a poor shielding material and provides only the mean value of $SE_T \approx 1.5$ dB in the EHF range. The coefficients of reflection, absorption, effective absorption, and transmission presented in Figure 5b for epoxy with 1.3 vol% quasi-1D fillers demonstrate the superior performance of the composites with quasi-1D fillers in the EHF band. Note that only 0.0002% of the incident EM wave is transmitted through the 1 mm thick film with only 1.3 vol% of quasi-1D $TaSe_3$ fillers. The shielding effectiveness of the same sample is shown in Figure 5c. Figure 5b,c indicates clearly that absorption is the dominant mechanism of the EMI shielding in the EHF range. This is different from the situation in the X-band where the reflection was substantial. The absorption SE_A increases from 55 to 75 dB as the frequency varies from 220 to 320 GHz. The EMI

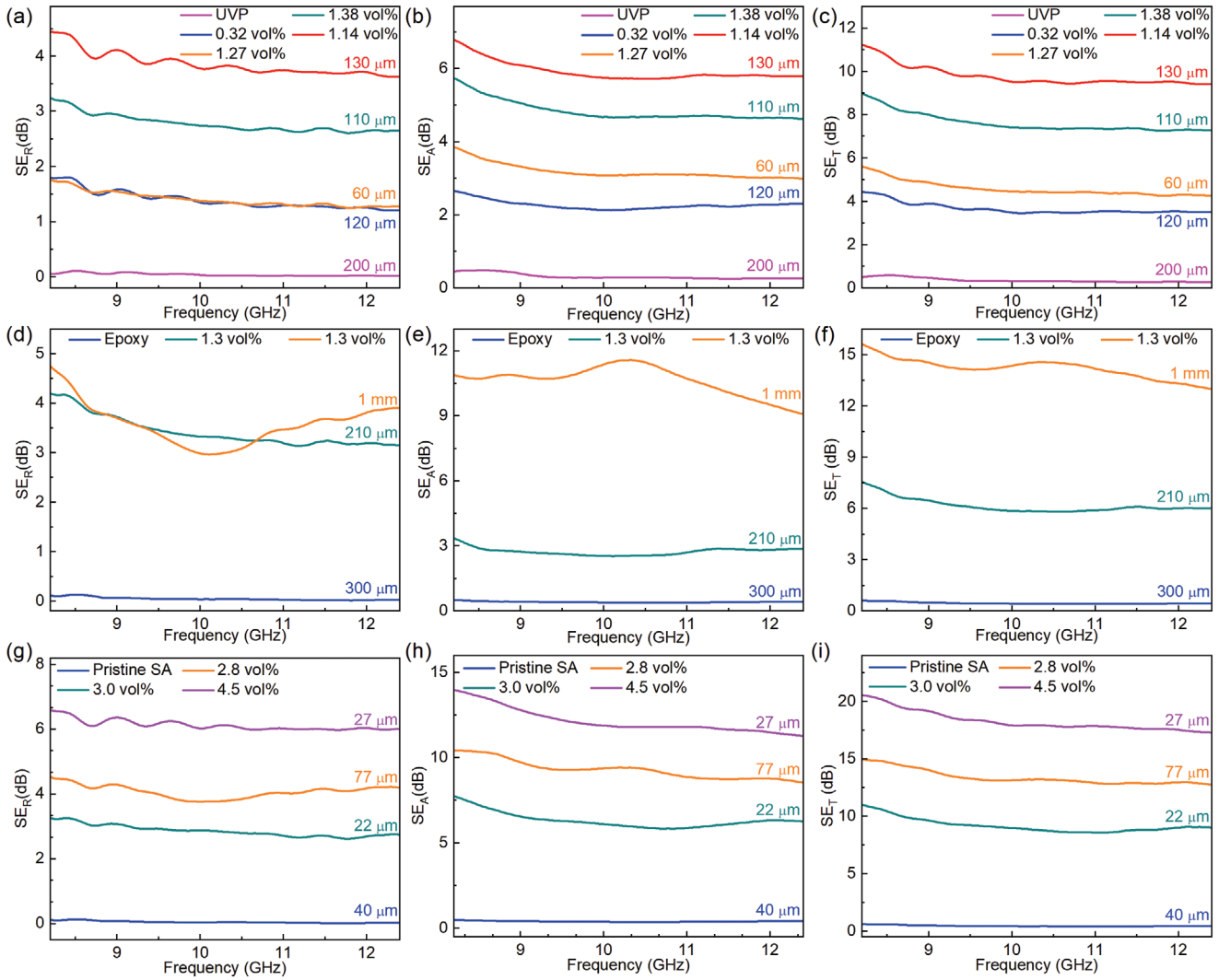

Figure 3. Electromagnetic characteristics of films with low concentration of quasi-1D $TaSe_3$ fillers in the X-band frequency range. a–i) Reflection (SE_R), absorption (SE_A), and total (SE_T) electromagnetic interference shielding effectiveness of: a–c) UV-cured polymer, d–f) epoxy, and g–i) sodium alginate films and composites with low concentration of quasi-1D $TaSe_3$ bundles of atomic threads as fillers. The concentration is indicated in the legends.

shielding by reflection contributes only ≈ 1.5 dB to the total shielding, and it slightly decreases from 1.7 to 1.4 dB as the frequency increases. Also, note that by adding only 1.3 vol% of quasi-1D fillers to the pristine epoxy, an enhancement of 50× in total shielding effectiveness in the EHF frequency range is achieved.

An important feature of the synthesized films is their electrical insulation. We verified that the DC electrical conductivity of the films with ≤3 vol% filler loading is below the instrumentation measurement limit. The upper bound of the electrical sheet resistance measurement capability of our instrument is $\approx 5 \times 10^{10}$ Ω. Thus, for samples with tens of micrometers thickness, the upper bound of measurable resistivity is $\approx 10^7$ Ω cm. This means that the loading fraction of the quasi-1D van der Waals fillers is below the percolation threshold. Experimenting with different loading fractions, we established that in the SA flexible film with 4.5 vol%, the electrical resistivity abruptly decreases to ≈5 Ω cm. The latter indicates that electrical percolation for the SA-based flexible films is achieved at filler concentration between 3 and 4.5 vol%. All other polymer base remained electrically insulating even when the loading fraction was reaching 4.5 vol%. The insulating nature of the films with the quasi-1D fillers is intriguing and clearly defined by unique properties of quasi-1D van der Waals materials. According to the conventional theories developed for carbon nanotubes and nanowires with high aspect ratio, the electrical percolation should be attained at even lower loading <1 vol%.[43–47] The disagreement with the known models can be explained by the fact that the conventional theories used the mathematical approximation of the fillers as straight cylinders, whereas we often observed $TaSe_3$ bending (see Figure 2), which could affect the percolation threshold. During material processing, we paid special attention to the uniformity of the filler dispersion and verified it with microscopy. Some deviation from the uniformity over the sample total area is a possible factor, which requires a separate investigation.

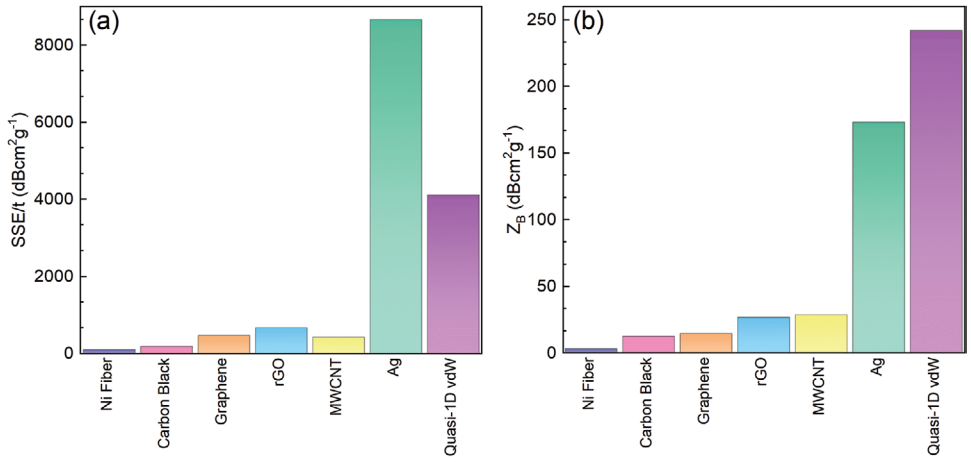

Figure 4. EMI shielding characteristics of polymeric composites with different fillers. a) The specific EMI shielding effectiveness normalized by thickness. A polymer composite with 90 wt% of Ag inclusion exhibit the highest SSE/*t*. b) The same plot in (a) normalized by the filler weight loading fraction. The Z_B factor indicates composite's shielding effectiveness per aerial density of the filler. The lower the thickness, density, and filler weight loading fraction and higher the total shielding effectiveness, the higher the Z_B. The data for other composites are from: Ni fiber,[39] carbon black,[40] graphene,[30] rGO,[41] MWCNT,[40] and Ag.[42]

Another interesting question is why electrically insulating films are so effective in blocking the EM waves. Even though the quasi-1D fillers do not create a percolated, electrically conductive network below 3 vol% concentration, they effectively couple with EM waves. The electric field of EM waves interacts with the free carriers in the quasi-1D conductors, and thus enables

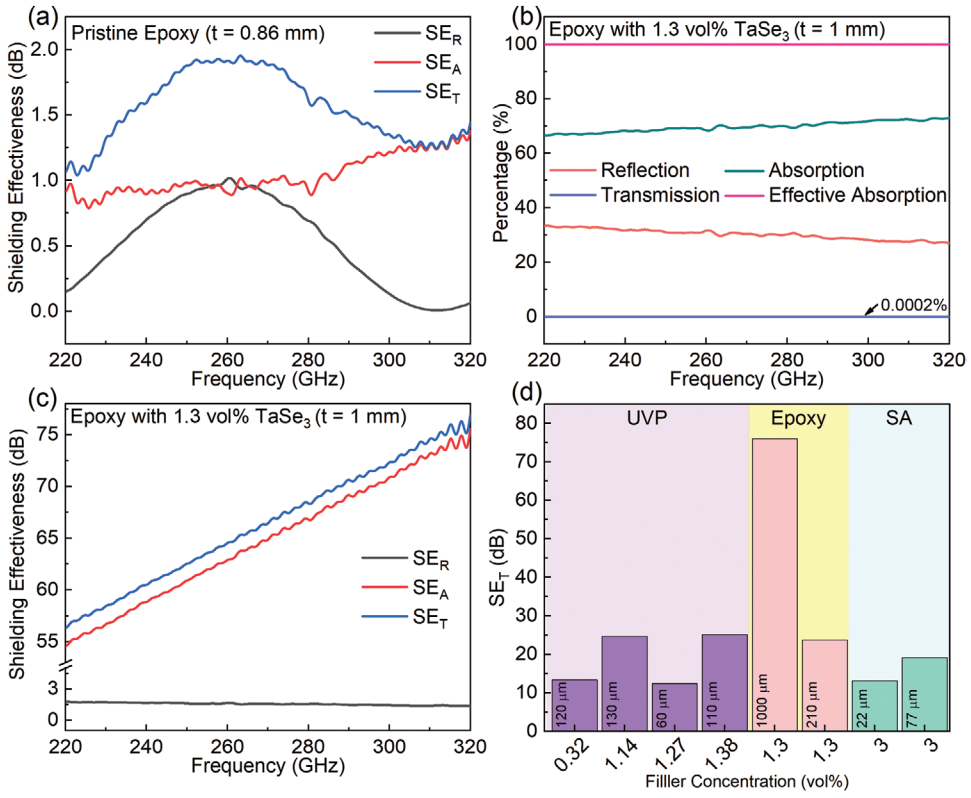

Figure 5. Electromagnetic shielding characteristics of the films with low concentration of quasi-1D $TaSe_3$ fillers in the EHF band. a) Shielding effectiveness of pristine epoxy used as the base material for some of the composites. b) Reflection, absorption, effective absorption, and transmission coefficients of epoxy with 1.3 vol% loading of the quasi-1D $TaSe_3$ fillers. Note that in the EHF range, almost all the incident EM wave energy is blocked and only 0.0002% is transmitted. c) Reflection, absorption, and total shielding effectiveness of the same composite. Note that absorption is the dominant mechanism in blocking the EM waves in the EHF band. d) Total shielding effectiveness of all samples tested in the EHF band. The results are shown for the frequency 320 GHz. The total shielding effectiveness scales with the loading fraction of quasi-1D fillers and the thickness of the films.

reflection and absorption of EM energy. Note that at the frequency of 10 GHz, the EM wavelength $\lambda = c/(\varepsilon_r^{1/2} f) \approx 19$ mm (here, $\varepsilon_r \approx 2.4$ is the relative dielectric constant of polymer base material). A few of connecting quasi-1D fillers with high aspect ratio would make something similar to an antenna, effective at receiving and re-emitting EM energy. A few connecting and bent quasi-1D fillers that form a circular loop would act similar to a magnetic antenna in this frequency range. These considerations can explain an efficiency of quasi-1D bundles of atomic threads as fillers in EMI shielding films. The "antenna" action in the X-band is consistent with the fact that reflection of EM waves made substantial contribution of the overall EMI shielding at these frequencies. In the EHF range, where the EM wavelength at $f = 300$ GHz is $\lambda \approx 0.65$ mm, the randomly distributed quasi-1D fillers can act more as the scattering objects, which explain the dominance of absorption in the overall EMI shielding.

One should point out that the electrical conduction properties of $TaSe_3$ itself are still not completely understood. Bulk $TaSe_3$ has not been studied in as much detail as other TMT materials, possibly due to its low superconducting phase transition $T_c \approx 2$ K.[15,48] A variety of measurements indicate that $TaSe_3$ is metallic or semimetallic down to T_c.[49–52] At the same time, some reports suggested that stress or strain can produce a semiconducting gap.[35,53] Moreover, many published studies on $TaSe_3$ do not include detailed compositional data (e.g., EDS, electron microprobe analysis, or inductively coupled plasma–mass spectrometry). At least some CVT-grown $TaSe_3$ crystals appear selenium deficient,[18,54] approximately $TaSe_{2.8}$, like the ones used in this work. Surprisingly, selenium-deficient $TaSe_3$ can be produced from even in selenium-rich CVT conditions.[34,55,56] Stoichiometric $TaSe_3$ has been isolated from high pressure conditions and selenium-flux growth.[33,57] Although selenium deficiency does not seem to affect the overall electrical conductivity of $TaSe_3$ or its T_c,[15,37,48,50–52] several studies indicate that doping can modify its electronic structure. For example, the mixed chalcogenide $Ta(S_xSe_{1-x})_3$ becomes semiconducting with increasing sulfur content,[58] and indium impurities from contacts to $TaSe_3$ can produce a metal–insulator transition.[59,60] In addition, the intercalation of copper into $TaSe_3$ causes T_c lowering and weak induced CDWs.[61] Further investigations clearly are needed to understand the impact of defects and dopants on the electrical properties of $TaSe_3$.

In conclusion, we demonstrated that quasi-1D van der Waals materials can be used as fillers in flexible polymer films providing excellent EMI shielding capability in the X-band and EHF-band. Polymer composites films (27 μm thickness) with only 4.5 vol% of quasi-1D $TaSe_3$ exfoliated atomic thread fillers delivered ≈ 20 dB of total EMI shielding in the practically important X-band GHz frequency range. The EMI shielding efficiency of the developed materials expressed via the total shielding effectiveness normalized by the mass density, thickness, and filler loading fraction, $Z_B \approx 242$ dB cm^{-2} g^{-1}, exceeds that of other polymers with various metallic, carbon nanotube, or graphene fillers. The EMI shielding performance of the films with the quasi-1D fillers in the EHF band of sub-THz frequencies was particularly impressive. Total shielding effectiveness SE_T changed from 60 dB to above 70 dB as the frequency varied from 240 to 320 GHz. This performance was achieved in composite films with only 1.3 vol% loading of exfoliated quasi-1D fillers of $TaSe_3$ and the film thickness of 1 mm. Interestingly, the efficient EMI shielding was achieved in polymer films, which retained their DC electrically insulating properties at loading less than 3 vol%, essential for many applications. The developed polymer films with quasi-1D fillers are promising for 5G-and-beyond communication technologies, which require electromagnetic shielding films, which are flexible, light-weight, corrosion resistive, electrically insulating, and inexpensive.

Experimental Section

Preparation of $TaSe_3$: 1.7315 g (9.57 mmol) of tantalum (STREM 99.98% purity) and 2.2718 g (28.8 mmol) of selenium (STREM 99.99% purity) were ground together gently with an agate mortar/pestle. This mixture was added to a 17.78 × 1 cm fused quartz ampule along with 62.3 mg iodine (J.T. Baker, 99.9% purity). The ampule was evacuated and backfilled with Ar three times while submerged in an acetonitrile/dry ice bath, and then flame sealed under vacuum. The ampule was placed in a Carbolite EZS 12/450B three-zone horizontal tube furnace and heated to 750–650 °C (source zone–growth zone) for 336 h. After the ampule had cooled to room temperature and was opened, the isolated shiny black crystals were left to sit in a fume hood for 1–2 h to allow excess iodine to sublime.

Polymer Composite Preparation: The bulk $TaSe_3$ crystals were added to acetone with a starting concentration of 0.5 mg mL^{-1} in 10 mL cylindrical vials and sonicated in a low power sonic bath (Branson 5510) for several hours. The vials were inspected visually every 2 h to verify the quality of the dispersion. The resultant dispersion was centrifuged (Eppendorf Centrifuge 5810) at 7000 rpm for 5 to 10 min. The supernatant was collected and poured in a Peltier dish to dry for characterization purposes. The precipitate, as well as some material stuck to the side walls of the vial after centrifugation, was collected and left in the ambient air until the solvent evaporated. The resulting dark brown, exfoliated $TaSe_3$ threads exhibited different aspect ratios (see Figures S3 and S4 in the Supporting Information for more optical microscopy and SEM images). The variation in aspect ratio of the $TaSe_3$ fillers is beneficial in EMI shielding applications and has been discussed in the text. The obtained fillers were mixed in precalculated proportions with three different off-the-shelf base polymeric matrices of UVP, SA, and epoxy. The UVP was mixed with low volume fraction of $TaSe_3$ at 500 rpm for 10 min using a high-shear speed mixer (Flacktek Inc.). The prepared mixture was sandwiched between two pieces of nylons and pressed gently until a thin film formed in between. The sandwich was left under the UV light for 2 min to cure. After that, the nylons were separated easily and a flexible film of UVP-$TaSe_3$ remained, as shown in Figure 1f. In case of SA-based flexible films, the SA powder was added to the deionized (DI) water, sealed, and stirred for 2 h on top of a hot plate with temperature set to 50 °C. Then, the $TaSe_3$ filler was added to the solution at low concentrations. The mixture was stirred and sonicated for 30 min and drop cast on a Peltier dish. The dish was placed on a hot plate at 50 °C for almost 1 h. The resultant was a dark brown flexible film shown in Figure 1g. The epoxy composites were made by mixing the epoxy resin (bisphenol-A-(epichlorhydrin), molecular weight ≤700, Allied High-Tech Products, Inc.) and hardener (triethylenetetramine, Allied High-Tech Products, Inc.) with the mass ratio of 100 to 12, respectively. The $TaSe_3$ filler was added afterward and mixed with the high-shear speed mixer at 500 rpm for 10 min. The compound was vacuumed for 10 min to remove the possible trapped air bubbles. The compound was mixed one more time at 300 rpm for 10 min, vacuumed, and then poured into special molds to cure. The product was the dark composite shown in Figure 1h. More details of the sample preparation are provided in the Supporting Information.

Mass Density Measurements: Using an electronic scale (Mettler Toledo), the weight of the samples was measured in air (w_a) and in DI water (w_w). In case of SA flexible films, the weights of the films were measured in air and ethanol (w_e) since SA is soluble in DI water. The

mass density of the samples were calculated according to Archimedes principle $\rho_c = (w_a/(w_a - w_{w,e})) \times (\rho_{w,e} - \rho_a) + \rho_a$ where ρ is the density and subscripts "a," "w," and "e" correspond to air, water, and ethanol, respectively. The volume fraction, φ, of the $TaSe_3$ filler was calculated according to the rule of mixtures as $\varphi = (\rho_c - \rho_p)/(\rho_f - \rho_p)$ where ρ_p and ρ_f are the density of the base polymer and $TaSe_3$ filler, respectively. The density values of each sample with its constituents are listed in the Supporting Information.

Electromagnetic Interference Shielding Measurements in the X-Band: To determine EMI characteristics, the scattering parameters, S_{ij}, were measured using the two-port PNA system. The indices i and j represent the ports, which are receiving and emitting the EM waves. Each port can simultaneously emit and detect the EM waves and thus the results of the measurements include four parameters of S_{11}, S_{12}, S_{21}, and S_{22}. Owing to the symmetry of the samples, one can expect that $|S_{11}| = |S_{22}|$ and $|S_{12}| = |S_{21}|$. The scattering parameters are related to the coefficients of reflection, $R = |S_{11}|^2$, and transmission, $T = |S_{21}|^2$. The measurements were performed in the X-Band frequency range (8.2–12.4 GHz) with the frequency resolution of 3 MHz. A PNA Keysight N5221A was used. The PNA was calibrated for 2-port measurements of scattering parameters S_{ij} at input power $P_{in} = 3$ dBm. A WR-90 commercial grade straight waveguide with two adapters at both ends with SMA coaxial ports was used as a sample holder. Special cables were used for high temperature RF measurements. The samples were a bit larger than the rectangular cross-section (22.8×10.1 mm^2) of the central hollow part of the waveguide in order to prevent the leakage of EM waves from the sender to receiver antenna. The scattering parameters, S_{ij}, were directly measured and used to extract the reflection and absorption shielding effectiveness of the composites.

Electromagnetic Interference Shielding Measurements in the EHF Band: Due to a small cross-section of the WR-3 waveguide, EMI characteristics in the sub-THz range were measured in free space. One of the most commonly used free-space techniques at THz and sub-THz frequencies is the time-domain spectroscopy (THz-TDS).[62] Its efficiency is limited to frequencies below 300 GHz due to the low power of the excitation signal in this spectral range.[63] Characterization of highly absorptive materials using THz-TDS may not be feasible. For this reason, the EMI shielding effectiveness was determined from the measured scattering parameters using Agilent N5245A vector network analyzer (VNA) with a pair of frequency extenders from Virginia Diodes Inc.[31,64] The quasi-optical path of the measurement setup consisted of two high-gain horn antennas and two double convex lenses to focus the EM wave on the sample under test. The measurements were performed in the frequency range from 220 to 320 GHz. The VNA with frequency extenders was calibrated using the Thru–Reflect–Line (TRL) method. The reference planes for 2-port measurements were achieved at the ends of the waveguide ports of both extenders. To compensate for the transmission losses in the measurement path, two additional reference measurements were performed. The measurement with an empty optical path and the measurement with a metal plate allow one to calculate the actual transmission and reflection coefficients, respectively. In order to improve the reliability of the collected data, additional time-domain gating was applied (see refs. [31,64–66] for more details).

Supporting Information

Supporting Information is available from the Wiley Online Library or from the author.

Acknowledgements

The work in the Balandin group was supported, in part, by the National Science Foundation (NSF) program Designing Materials to Revolutionize and Engineer our Future (DMREF) via a project DMR-1921958 entitled Collaborative Research: Data Driven Discovery of Synthesis Pathways and Distinguishing Electronic Phenomena of 1D van der Waals Bonded Solids; the Semiconductor Research Corporation (SRC) contract 2018-NM-2796 entitled One-Dimensional Single-Crystal van der Waals Metals: Ultimately Downscaled Interconnects with Exceptional Current-Carrying Capacity and Reliability; and by the Proof of Concept (POC) project of the Office of Technology Partnerships (OTP), University of California, Riverside (UCR). S.R. and Y.Y. acknowledge support from the CENTERA Laboratories in the framework of the International Research Agendas Program for the Foundation for Polish Sciences cofinanced by the European Union under the European Regional Development Fund (No. MAB/2018/9). Z.B. and F.K. thank Amirmahdi Mohammadzadeh and Dylan Wright, POEM Center, UCR, for assistance with SEM characterization.

Conflict of Interest

The authors declare no conflict of interest.

Author Contributions

A.A.B. and F.K. conceived the idea of the electromagnetic shielding films with quasi-1D fillers and planned the study. A.A.B. and F.K. coordinated the project and contributed to the experimental data analysis. Z.B. exfoliated the material, prepared the composites, performed measurements in the X-band frequency range, and analyzed the experimental data. Y.G. synthesized bulk crystals and conducted material characterization. S.G. conducted Raman spectroscopy of exfoliated materials and thin films. S.B. conducted SEM characterization. T.T.S. supervised material synthesis and contributed to data analysis. A.A.B. and F.K. led the manuscript preparation. Y.Y. and K.G. carried out measurements in the EHF frequency range and processed experimental data using the time-domain gaiting method. G.C. and S.R. contributed to data analysis and interpretation. All authors contributed to writing and editing of the manuscript.

Keywords

electromagnetic interference shielding, GHz and sub-THz, polymer composites, quasi-1D materials, van der Waals materials

Received: October 24, 2020
Revised: December 10, 2020
Published online:

[1] K. S. Novoselov, A. K. Geim, S. V. Morozov, D. Jiang, Y. Zhang, S. V. Dubonos, I. V. Grigorieva, A. A. Firsov, *Science* **2004**, *306*, 666.
[2] Y. Zhang, Y.-W. Tan, H. L. Stormer, P. Kim, *Nature* **2005**, *438*, 201.
[3] A. A. Balandin, *Nat. Mater.* **2011**, *10*, 569.
[4] A. K. Geim, I. V. Grigorieva, *Nature* **2013**, *499*, 419.
[5] A. A. Balandin, *Nat. Nanotechnol.* **2013**, *8*, 549.
[6] M. A. Stolyarov, G. Liu, M. A. Bloodgood, E. Aytan, C. Jiang, R. Samnakay, T. T. Salguero, D. L. Nika, S. L. Rumyantsev, M. S. Shur, K. N. Bozhilov, A. A. Balandin, *Nanoscale* **2016**, *8*, 15774.
[7] A. Geremew, M. A. Bloodgood, E. Aytan, B. W. K. Woo, S. R. Corber, G. Liu, K. Bozhilov, T. T. Salguero, S. Rumyantsev, M. P. Rao, A. A. Balandin, *IEEE Electron Device Lett.* **2018**, *39*, 735.
[8] T. A. Empante, A. Martinez, M. Wurch, Y. Zhu, A. K. Geremew, K. Yamaguchi, M. Isarraraz, S. Rumyantsev, E. J. Reed, A. A. Balandin, L. Bartels, *Nano Lett.* **2019**, *19*, 4355.
[9] M. A. Bloodgood, P. Wei, E. Aytan, K. N. Bozhilov, A. A. Balandin, T. T. Salguero, *APL Mater.* **2018**, *6*, 026602.

[10] X. Liu, J. Liu, L. Y. Antipina, J. Hu, C. Yue, A. M. Sanchez, P. B. Sorokin, Z. Mao, J. Wei, *Nano Lett.* **2016**, *16*, 6188.
[11] H. Yi, T. Komesu, S. Gilbert, G. Hao, A. J. Yost, A. Lipatov, A. Sinitskii, J. Avila, C. Chen, M. C. Asensio, P. A. Dowben, *Appl. Phys. Lett.* **2018**, *112*, 052102.
[12] A. Lipatov, M. J. Loes, H. Lu, J. Dai, P. Patoka, N. S. Vorobeva, D. S. Muratov, G. Ulrich, B. Kästner, A. Hoehl, G. Ulm, X. C. Zeng, E. Rühl, A. Gruverman, P. A. Dowben, A. Sinitskii, *ACS Nano* **2018**, *12*, 12713.
[13] G. Cheon, K.-A. N. Duerloo, A. D. Sendek, C. Porter, Y. Chen, E. J. Reed, *Nano Lett.* **2017**, *17*, 1915.
[14] A. K. Geremew, S. Rumyantsev, M. A. Bloodgood, T. T. Salguero, A. A. Balandin, *Nanoscale* **2018**, *10*, 19749.
[15] S. Nagata, S. Ebisu, T. Aochi, Y. Kinoshita, S. Chikazawa, K. Yamaya, *J. Phys. Chem. Solids* **1991**, *52*, 761.
[16] B. J. Kim, B. J. Jeong, S. Oh, S. Chae, K. H. Choi, T. Nasir, S. H. Lee, H. K. Lim, I. J. Choi, M.-K. Hong, H. K. Yu, J.-H. Lee, J.-Y. Choi, *Materials* **2019**, *12*, 2462.
[17] A. I. U. Saleheen, R. Chapai, L. Xing, R. Nepal, D. Gong, X. Gui, W. Xie, D. P. Young, E. W. Plummer, R. Jin, *npj Quantum Mater.* **2020**, *5*, 53.
[18] J. Yang, Y. Q. Wang, R. R. Zhang, L. Ma, W. Liu, Z. Qu, L. Zhang, S. L. Zhang, W. Tong, L. Pi, W. K. Zhu, C. J. Zhang, *Appl. Phys. Lett.* **2019**, *115*, 033102.
[19] J. P. Gogoi, A. Shabir, *Materials for Potential EMI Shielding Applications*, Elsevier, Amsterdam, The Netherlands **2020**, pp. 379–390.
[20] R. M. Simon, *Polym.-Plast. Technol. Eng.* **1981**, *17*, 1.
[21] F. Shahzad, M. Alhabeb, C. B. Hatter, B. Anasori, S. Man Hong, C. M. Koo, Y. Gogotsi, *Science* **2016**, *353*, 1137.
[22] D. Jiang, V. Murugadoss, Y. Wang, J. Lin, T. Ding, Z. Wang, Q. Shao, C. Wang, H. Liu, N. Lu, R. Wei, A. Subramania, Z. Guo, *Polym. Rev.* **2019**, *59*, 280.
[23] D. Wanasinghe, F. Aslani, G. Ma, D. Habibi, *Nanomaterials* **2020**, *10*, 541.
[24] D. D. Chung, *Carbon* **2001**, *39*, 279.
[25] Z. Chen, C. Xu, C. Ma, W. Ren, H.-M. Cheng, *Adv. Mater.* **2013**, *25*, 1296.
[26] N. Yousefi, X. Sun, X. Lin, X. Shen, J. Jia, B. Zhang, B. Tang, M. Chan, J.-K. Kim, *Adv. Mater.* **2014**, *26*, 5480.
[27] B. Shen, W. Zhai, W. Zheng, *Adv. Funct. Mater.* **2014**, *24*, 4542.
[28] D.-X. Yan, H. Pang, B. Li, R. Vajtai, L. Xu, P.-G. Ren, J.-H. Wang, Z.-M. Li, *Adv. Funct. Mater.* **2015**, *25*, 559.
[29] F. Kargar, Z. Barani, M. Balinskiy, A. S. Magana, J. S. Lewis, A. A. Balandin, *Adv. Electron. Mater.* **2019**, *5*, 1800558.
[30] Z. Barani, F. Kargar, A. Mohammadzadeh, S. Naghibi, C. Lo, B. Rivera, A. A. Balandin, *Adv. Electron. Mater.* **2020**, *6*, 2000520.
[31] Z. Barani, F. Kargar, K. Godziszewski, A. Rehman, Y. Yashchyshyn, S. Rumyantsev, G. Cywiński, W. Knap, A. A. Balandin, *ACS Appl. Mater. Interfaces* **2020**, *12*, 28635.
[32] S. Nie, L. Xing, R. Jin, W. Xie, Z. Wang, F. B. Prinz, *Phys. Rev. B* **2018**, *98*, 125143.
[33] W. Xia, X. Shi, Y. Zhang, H. Su, Q. Wang, L. Ding, L. Chen, X. Wang, Z. Zou, N. Yu, L. Pi, Y. Hao, B. Li, Z. Zhu, W. Zhao, X. Kou, Y. Guo, *Phys. Rev. B* **2020**, *101*, 155117.
[34] Y. Zhang, T. Zhu, H. Bu, Z. Cai, C. Xi, B. Chen, B. Wei, D. Lin, H. Xie, M. Naveed, X. Xi, F. Fei, H. Zhang, F. Song, *AIP Adv.* **2020**, *10*, 095314.
[35] J. Á. Silva-Guillén, E. Canadell, *2D Mater.* **2020**, *7*, 025038.
[36] G. Liu, S. Rumyantsev, M. A. Bloodgood, T. T. Salguero, M. Shur, A. A. Balandin, *Nano Lett.* **2017**, *17*, 377.
[37] E. Bjerkelund, A. Kjekshus, *Z. Anorg. Allg. Chem.* **1964**, *328*, 235.
[38] Q. Wei, S. Pei, X. Qian, H. Liu, Z. Liu, W. Zhang, T. Zhou, Z. Zhang, X. Zhang, H. Cheng, W. Ren, *Adv. Mater.* **2020**, *32*, 1907411.
[39] X. Shui, D. D. L. Chung, *J. Electron. Mater.* **1997**, *26*, 928.
[40] M. H. Al-Saleh, U. Sundararaj, *Carbon* **2009**, *47*, 1738.
[41] N. Agnihotri, K. Chakrabarti, A. De, *RSC Adv.* **2015**, *5*, 43765.
[42] C. Liang, K. Ruan, Y. Zhang, J. Gu, *ACS Appl. Mater. Interfaces* **2020**, *12*, 18023.
[43] A. Celzard, J. F. Marêché, F. Payot, *J. Phys. D: Appl. Phys.* **2000**, *33*, 1556.
[44] C. L. Huang, Y. J. Wang, Y. C. Fan, C. L. Hung, Y. C. Liu, *J. Mater. Sci.* **2017**, *52*, 2560.
[45] X. Xia, Y. Wang, Z. Zhong, G. J. Weng, *J. Appl. Phys.* **2016**, *120*, 085102.
[46] R. Ram, D. Khastgir, M. Rahaman, *Polym. Int.* **2019**, *68*, 1194.
[47] Y. Pan, G. J. Weng, S. A. Meguid, W. S. Bao, Z. H. Zhu, A. M. S. Hamouda, *J. Appl. Phys.* **2011**, *110*, 123715.
[48] T. Sambongi, M. Yamamoto, K. Tsutsumi, Y. Shiozaki, K. Yamaya, Y. Abe, *J. Phys. Soc. Jpn.* **1977**, *42*, 1421.
[49] E. Bjerkelund, J. H. Fermor, A. Kjekshus, *Acta Chem. Scand.* **1966**, *20*, 1836.
[50] P. Haen, P. Monceau, B. Tissier, G. Waysand, A. Meerschaut, P. Molinie, J. Rouxel, *Ferroelectrics* **1977**, *17*, 447.
[51] H. P. Geserich, G. Scheiber, F. Lévy, P. Monceau, *Physica B+C* **1986**, *143*, 174.
[52] T. Sambongi, M. Ido, K. Tsutsumi, M. Yamamoto, T. Takoshima, Y. Abe, in *Quasi One-Dimensional Conductors I* (Eds: S. Barišić, A. Bjeliš, J. R. Cooper, B. A. Leontić), Lecture Notes in Physics, Springer, Berlin, Germany **1979**, pp. 349–353.
[53] T. M. Tritt, R. L. Jacobsen, A. C. Ehrlich, D. J. Gillespie, *Phys. B* **1994**, *194–196*, 1303.
[54] S. Kikkawa, K. Shinya, M. Koizumi, *J. Solid State Chem.* **1982**, *41*, 323.
[55] T. M. Tritt, E. P. Stillwell, M. J. Skove, *Phys. Rev. B* **1986**, *34*, 6799.
[56] G. Kumagai, T. Matsuura, K. Ichimura, S. Tanda, *J. Phys.: Conf. Ser.* **2009**, *150*, 052134.
[57] S. Kikkawa, N. Ogawa, M. Koizumi, Y. Onuki, *J. Solid State Chem.* **1982**, *41*, 315.
[58] K. Yamaya, Y. Abe, *Mol. Cryst. Liq. Cryst.* **1982**, *81*, 133.
[59] J. Gill, *Phys. Rev. B: Condens. Matter Mater. Phys.* **1996**, *53*, 15586.
[60] A. V. Zavalko, S. V. Zaitsev-Zotov, *J. Phys. IV* **2005**, *131*, 359.
[61] A. Nomura, K. Yamaya, S. Takayanagi, K. Ichimura, S. Tanda, *EPL* **2018**, *124*, 67001.
[62] M. Zdrojek, J. Bomba, A. Lapińska, A. Dużyńska, K. Żerańska-Chudek, J. Suszek, L. Stobiński, A. Taube, M. Sypek, J. Judek, *Nanoscale* **2018**, *10*, 13426.
[63] M. Naftaly, *IEEE Sens. J.* **2012**, *13*, 8.
[64] Y. Yashchyshyn, K. Godziszewski, *IEEE Trans. Terahertz Sci. Technol.* **2018**, *8*, 19.
[65] N. Dvurechenskaya, P. R. Bajurko, R. J. Zieliński, Y. Yashchyshyn, *Metrol. Meas. Syst.* **2013**, *21*, 217.
[66] K. Godziszewski, Y. Yashchyshyn, in *2016 21st Int. Conf. on Microwave, Radar and Wireless Communications (MIKON)*, IEEE, Piscataway, NJ, USA **2016**, https://doi.org/10.1109/MIKON.2016.7491939.